Romanian Reports in Physics, Vol. 66, No. 3, P. 862–876, 2014

ANNUAL DOSE RATE DETERMINATION BY HIGH RESOLUTION GAMMA SPECTROMETRY FOR TL DATING OF LOESS DEPOSITS IN SOUTH-EASTERN DOBRUDJEA, ROMANIA

L.C. TUGULAN[1*], O.G. DULIU[2]

[1]University of Bucharest, Doctoral School on Physics,
405, Atomiştilor str., P.O. Box MG-11, RO-077125, Măgurele (Ilfov), Romania, EU
E-mail: lctugulan@yahoo.com
[2]University of Bucharest, Department of Structure of Matter,
Earth and Atmospheric Physics and Astrophysics,
405, Atomiştilor str., P.O. Box MG-11, RO-077125 Măgurele (Ilfov), Romania, EU
E-mail: duliu@b.astral.ro

Received April 22, 2013

Abstract. A method to determine the background annual dose rates for further dating of loess deposits is detailed presented. The proposed method can identify the contributions of any radionuclide belonging to the natural radioactive series as well those of the ^{40}K by taking into account the overlapping gamma ray spectral lines. Before to be applied on loess samples, the method was checked on the IAEA-RGTh-1 reference material, giving a good agreement between certified IAEA-RGTh-1 values and our determinations, *i.e.*, $t = -0.011$ for a paired t-test at $p > 0.991$. Applied to loses collected from different horizons, it was possible not only to calculate the annual dose rates, whose values ranged between 2.49 and 3.19 mGy/y but also to evidence that in all samples, regardless their position within loess deposit, all three natural radioactive series were in secular equilibrium.

Key words: Annual dose rate, Gamma ray spectrometry, Natural radioactivity, Loess age.

PACS: 78.60.Kn, *91.80.Wx

1. INTRODUCTION

Loess represents a type of aeolian, loosely cemented sediments, accumulated in huge deposits all over the word, mainly during the Pleistocene glaciations. The relative younger ages of loess deposits, a sporadic presence of tefra layers as well as a relative homogeneity of its geochemistry make loess absolute dating a relative difficult task. Only absolute geochronology methods based on the accumulation of radiation defects such as Thermoluminicence (TL), or Optical or Infrared Stimulated Luminescence (O/IRS) together with Palaeomagnetism gave robust ages for a differ-

*Permanent address: National Institute for Physics and Nuclear Engineering "Horia Hulubei", 30, Reactorului str., P.O. Box MG-6, RO-077125 Măgurele, Ilfov, Romania, EU

ent loess deposits [1–6].

At its turn, TL is a phenomenon linked to the formation of radiation defects in insulating solids. As the amount of TL radicals is proportional with the absorbed dose, beginning with early 1964, TL has been used in archaeology [7–9] as well as in geology [10, 11] as an absolute dating method. Techniques and methods used in dating by thermoluminescence were reviewed by Aitken in an excellent introduction book [12]. Accordingly, the geologic age *A(t)* of soil or sediments is

$$A(t) = \frac{D_e}{D'}, \tag{1}$$

where: D_e is the total dose accumulated (paleodose) and D' is the annual radiation dose rate.

Annual dose rates are due to materials exposure to natural radiations sources such as natural radioactive series of ^{232}Th, ^{238}U, and ^{235}U as well as natural ^{40}K and ^{87}Rb to which the cosmic radiation should be add [13]. For this reason, an accurate determination of the annual dose rates represents one of the most important stages in TL dating.

By taking also into account the different sources of radiation which could induce TL centres, the annual dose rate D' could be describe, according to Ref. [12], by the relation:

$$D' = a\frac{D'(\alpha)}{1+1.5WF} + b\frac{D'(\beta)}{1+1.25WF} + g\frac{D'(\gamma)}{1+1.14WF} + D_c \tag{2}$$

where: *a*, *b* and *g* represents the alpha, beta and respectively gamma rays radiations efficiency in producing TL centers, $D'(\alpha)$, $D'(\beta)$, and $D'(\gamma)$ are partial dose-rates due to alpha, beta and respectively gamma rays, D_c is cosmic radiation dose rate, *W* represents the saturation content for loess samples F is a factor that quantifies the

Table 1

The main characteristics (Chr.) of loess/paleo-soil samples

Sample	Depth (m)	Chr.	Sample	Depth (m)	Chr.
G 1-2 (paleo-soil)	4.5	light - brown	G 5 (loess)	10.1	dark red brow
G 2 (loess)	5.1	fawn brown	G 5-6 (paleo-soil)	10.4	dark brown
G 3 (loess)	8.2	light tan brown	G 6 (loess)	10.9	red brown
G 4 (loess)	9.1	dark red brown	G 7 (loess)	11.8	red brown
G 4-5 (paleo-soil)	9.5	brown	G 8 (paleo-soil)	19.1	red brown

relative period of time during which a sample was saturated with water.

At the same time, the partial dose rates of alpha, beta and gamma rays are strictly determined by the content of natural radioactive elements, so that a correct estimation of their content is of extreme importance for a confident TL dating. Among the existing methods used for this purpose, gamma ray spectrometry, due to its noninvasive character, seems to be one of the most suitable [14–17]. As this method could be used by a specialized gamma spectrometry laboratory, we have decided to utilize this techniques to determine with high accuracy and precision the content of natural radioactive elements as a compulsory step for the future TL age measurements of Dobrudjea's loess deposits.

Accordingly, our results concerning the annual dose rates in loess deposits will be presented and discussed in this paper.

2. MATERIALS AND METHODS

2.1. LOESS AND PALEO-SOIL SAMPLES

Ten loess and paleo-soil samples were collected from a 20 m thick loess deposit South of the Costinesti city (South-Eastern Dobrudjea). About 2 kg of soil was hand picked by using 30 cm metallic corers. A short description of samples is reproduced in Table 1.

2.2. HIGH RESOLUTION GAMMA SPECTROMETRY

All radiometric measurements have been performed by using a CANBERRA REGe type detector (ISOCS characterization) equipped with a 0.6 mm thick carbonepoxy window and a DSA 1000 multichannel analyser. The detector relative efficiency was of 40% and an energy resolution of 1.96 keV for the 1332 keV line of ^{60}Co and of 0.89 keV for the 122 keV line of ^{57}Co. To reduce the background, the detector was placed inside a 747 Canberra lead shield. Gamma spectra were processed by using the GENIE 2000 software. The detector efficiency calibration, self-absorption correction and coincidence-summing correction was done with Lab-SOCS (Cannbera) software.

Samples, dried at constant mass of about 1100 g, were placed in 130G hermetically closed Marinelli beakers and stored for 28 days for radioactive equilibrium. After that, the gamma-spectrum of each sample was two recorded for 360,000 s. To check the measurements accuracy we have used the standard reference material IAEA-RGTh-1 [18]. To avoid the radon accumulation in the vicinity of detector, all measurements were performed only in working days when the laboratory ventilation worked non-stop.

Table 2

The gamma ray energies (E_γ) of ^{228}Ac, ^{212}Bi and ^{208}Tl used to determine the activity concentrations of the ^{232}Th series member as well as the most significant interferences.

Nuclide	$T_{1/2}$	E_γ (keV)	I_γ (%)	Possible interferences		
				Nuclide	E_γ (keV)	I_X or I_γ (%)
^{228}Ac	6.15 h	209.25	3.89	^{234m}Pa	209.90	0.0131
		409.46	1.92	^{235}U	410.29	0.0380
				^{231}Pa	410.30	0.0032
		772.29	1.49	^{227}Th	773.00	0.00012
		794.95	4.25	^{235}U	794.70	0.0006
		835.71	1.61	no interferences		
		911.20	25.8	^{227}Th	910.00	0.000011
		968.97	15.8	^{227}Th	970.00	0.000028
		1630.63	1.51	no interferences		
^{212}Bi	60.6 m	727.33	6.58	^{228}Ac	726.86	0.620
		1620.50	1.49	no interferences		
^{208}Tl	3.05 m	583.19	84.5	^{228}Ac	583.41	0.111
				^{231}Pa	583.00	0.00442
		763.13	1.81	^{227}Th	762.2	0.00025
		860.56	12.42	no interferences		

I_X and I_γ stand for X and γ ray emission probabilities

As the Marinelli 130G vessel geometry is predefined in the LabSOCS software, we consider variable only the sample height and the vessel position on the detector. The estimated value of the height relative uncertainty was of 1.0 % while in the case of Marinelli vessel positioning with respect to detector axis the relative uncertainty was of 1.5 %.

In all cases we have determined or computed the peak area, background peak area, source-detector distance as well as sample geometry, sample self attenuation variation as well as the coincidence summing correction factor.

The activity concentration of ^{40}K have been determined by the 1460.83 keV line. Further, we have estimated the activity concentration of ^{87}Rb by assuming and activities ratio of ^{87}Rb/^{40}K of 0.142 [19].

The branching as well as the energy released by the ^{232}Th, ^{238}U and ^{235}U series member were those reported by Gurin *et al.* [20] by considering the radioactive equilibrium in both pre-Rn and post-Rn subseries. At the same time, the activity concentrations were calculated from naturals decay series of pre and post Rn by its weighted averages.

Table 3

The gamma ray energies (E_γ) of ^{234m}Pa, ^{230}Th, ^{214}Bi and ^{210}Pb used to determine the activity concentrations of the ^{238}U series member as well as the most significant interferences.

Nuclide	$T_{1/2}$	E_γ (keV)	I_γ (%)	Possible interferences		
				Nuclide	E_γ (keV)	I_X or I_γ (%)
^{234m}Pa	1.17 m	1001.03	0.837	^{228}Ac	1000.69	0.005
				^{227}Th	999.8	0.000028
^{230}Th	75.4 ky	67.67	0.377	^{231}Th	68.48	0.0057
^{214}Bi	19.9 m	768.36	4.94		no interferences	
		806.17	1.22	^{234m}Pa	805.80	0.0043
				^{227}Th	807.50	0.000047
		934.06	3.03		no interferences	
		1120.29	15.1	^{234m}Pa	1120.60	0.0017
				^{214}Bi	1118.90	0.04
		1661.28	1.15		no interferences	
		1729.60	2.92		no interferences	
		1764.49	15.4	^{234m}Pa	1765.44	0.00868
		1847.42	2.11		no interferences	
^{210}Pb	22.3 y	46.54	4.25	^{231}Pa	46.36	0.223

In these conditions, we have estimated sample heterogeneities at 2.5 %. The weight uncertainty, those of correction factor for the coincidence summing as well as those arising from the spectral interferences at 0.5 %, 3.0 % and 6.5 % respectively.

2.3. NATURAL RADIOACTIVE SERIES AS WELL AS ^{40}K MEASUREMENTS

The major problem in determining radiometrically the actinide content of a chosen material by analysing its gamma ray spectrum consists of a correct identification of the multitude of possible interferences which exist. For this reason, in Table 2 to 5 we have reproduced the lists of all identified interferences whose influence on the final results was taken into account when we calculated the final contented of natural radionuclies in loess samples. It is worth mentioning that all interferences were calculated and corrected by using the GENIE software, based on the nuclear data of Ref [21].

We have performed such correction in the case of both ^{238}U and ^{235}U series as well as in the case of ^{40}K. In all cases, the main interfering isotopes were ^{228}Ac and ^{234m}Pa whose contribution was deduced from the experimental gamma spectrum line after were corrected for coincidence summing and detector efficiency, including self-absorption [22, 23].

Table 4

The ^{235}U series radionuclides with their representative gamma energies E_γ and possible spectral interference.

Nuclide	$T_{1/2}$	E_γ (keV)	I_γ (%)	Possible interferences		
				Nuclide	E_γ (keV)	I_X or I_γ (%)
^{235}U	704 My	185.71	57.2	^{228}Ac	184.54	0.07
				^{234}Th	184.80	0.013
				^{234m}Pa	184.70	0.0017
				^{226}Ra	186.21	3.59
				^{227}Th	184.65	0.0038
^{231}Th	25.5 h	25.65	14.5	^{231}Pa	25.51	0.117
^{219}Rn	3.96 s	401.81	6.374	no interferences		

2.3.1. The ^{232}Th natural radioactive series

In the Table 2, we have reproduced the energies of the representative gamma line of the ^{232}Th series together with the most significant spectral interferences. All these data were used to determine not only the activity concentration of ^{232}Th, but also those of of ^{212}Bi and ^{208}Tl, establishing in this way the existence of the radioactive equilibrium within Thorium radioactive series.

In the case of ^{232}Th series, the activity concentrations were calculated by taking into account the gamma spectra of ^{228}Ac, ^{212}Pb as well as those of ^{208}Tl.

Accordingly, in the case of ^{228}Ac we have considered the following gamma - ray energies: 209.25 keV, 409.46 keV, 772.29 keV, 794.95 keV, 835.71 keV, 911.20 keV, 968.97 keV and 1630.63 keV, considered free of other interferences or whose interferences, as Table 2 shows, could be considered as negligible.

The ^{212}Bi activity concentration was determined by means of its 1620.50 keV lines which shows no interferences. To determine the ^{208}Tl activity concentration we have measured the 763.13 keV and 860.56 keV gamma ray lines. The peak at 763.13 keV interfere with gamma emission at 762.20 keV of ^{227}Th (^{235}U series), which is negligible while the 860.56 keV peak does not present any interferences.

2.3.2. The ^{238}U natural radioactive series

As in previous case, on Table 2 we have reproduced the energies of gamma-ray of ^{238}U daughters used to determine experimentally the activity concentrations of entire ^{238}U series.

Accordingly, the activity concentrations were calculated by using the following gamma-ray lines: ^{234m}Pa (1001.03 keV), ^{230}Th (67.67 keV), ^{214}Bi (768.36, 806.17, 934.06, 1120.29, 1661.28, 1729.60, 1764.49 and 1847.42 keV) as well as

^{210}Pb (46.54 keV).

As the 1001.03 keV line of ^{234m}Pa interferes with the 1000.69 keV line of ^{228}Ac and the 998.8 keV line of ^{227}Th, its real intensity was calculated by subtracting from the experimental line $Ac^{911,20}_{228,exp}$ the contribution of the ^{228}Ac 1000.69 keV line following the relation:

$$Pa^{1001.03}_{234m} = Pa^{1001.03}_{234m,exp} - Ac^{911,20}_{228,exp} \cdot \frac{(I_\gamma \epsilon F_C)_{1000.69}}{(I_\gamma \epsilon F_C)_{911.20}} \tag{3}$$

where: I_γ represents the emission probability of gamma ray, ϵ is the corresponding detector efficiency including self-absorption correction while F_c stays for coincidence summing factor.

As the other lines present no interferences, it was possible to calculate the activity concentration of post-radon member of ^{238}U series, establishing in this way at which extent the ^{238}U could be considered in radioactive equilibrium.

2.3.3. ^{235}U series measurements

As in previous cases, the activity concentrations of ^{235}U series were calculated by means of more lines such as 185.71 keV, ^{235}U, 25.65 keV ^{231}Th and 401.81 keV ^{219}Rn.

Regarding 185.71 keV line of ^{235}U, the corresponding activity concentration was calculated by taking into account the interferences due to ^{228}Ac line of 184.45 keV, ^{234}Th line of 184.80 keV and ^{226}Ra line of 186.21, (both of them by means of ^{234m}Pa line of 1001.03 keV), following the relation:

$$\begin{aligned} U^{185.71}_{235} = U^{185.71}_{235,exp} - Ac^{911.20}_{228,exp} \cdot \frac{(I_\gamma \epsilon F_C)_{184.54}}{(I_\gamma \epsilon F_C)_{911.20}} - \\ - Pa^{1001.03}_{234m,exp} \cdot \frac{(I_\gamma \epsilon\, F_C)_{184.80}}{(I_\gamma \epsilon - F_C)_{1001.03}} - \\ - Pa^{1001.03}_{234m,exp} \cdot \frac{(I_\gamma \epsilon F_C)_{186.21}}{(I_\gamma \epsilon - F_C)_{1001.03}} \end{aligned} \tag{4}$$

In this case, we have neglected the interferences due to ^{234m}Pa line of 184.70 keV as well as those of 184.65 keV due to ^{237}Th, as both of them have negligible intensities.

2.3.4. ^{40}K measurements

The unique gamma line of ^{40}K (1460.83 keV and 11 % emission probability) shows an interference with the ^{228}Ac line of 1459.14 keV and an emission probability of 0.83 %. Accordingly, the net activity concentration of of ^{40}K was calculated by following en equation similar to eq. (3):

$$K_{40}^{1460.83} = K_{40,exp}^{1460.83} - Ac_{228,exp}^{911,20} \cdot \frac{(I_\gamma \epsilon F_C)_{1459.14}}{(I_\gamma \epsilon F_C)_{911.20}} \quad (5)$$

3. RESULTS AND DISCUSSION

Before computing the annual dose rate, we have checked the accuracy of the gamma spectrometric method used in the case of loess-paleo-soil samples by investigating, in the same condition, the IAEA-RGTh-1 reference material [18] due to the fact that the interferences of uranium series by the thorium series gamma emissions could not be neglected. The results thus obtained are reproduce din Table 5.

As it can be observed from these data, we have obtained in the case of all natural radioactive series a discrepancy of maximum 3 %, which, in the case of ^{40}K reached about 9 %. By taking into account that in this case, the Thorium content was dominant with respect with other radioactive elements, we could consider that the radiometric determination of the activity concentration is enough accurate to be used for further loess as well as paleo-soil determination.

The same experimental determinations of the IAEA-RGTh-1 reference material gave for the ^{238}U/^{235}U activity concentrations ratio a value of 22.2 $\pm$ 0.5, coincident within experimental uncertainties with the value of 21.72 $\pm$ 0.03 value recommended by IUPAC database [23], once more confirming the accuracy of our measurements. Moreover, a paired t-test applied on both certified and measured values gave a *t* value of -0.011 at $p > 0.991$, confirmed the quality of our determinations as well as the fact that the gamma spectroscopy represents a confident method in determining the activity concentration of the main radioactive element, an compulsory stage for any TL or OSL age determination.

Table 5

The activity concentrations - measured and certified - of IAEA-RGTh-1 reference material for the same experimental conditions as for gave for *t* parameter a value of -0.011 at $p > 0.991$.

Radionuclide	Experimental values (Bq/kg)	Certified values (Bq/kg)	Difference (%)
^{232}Th, full series	3223 $\pm$ 226	3250 $\pm$ 90	-0.83
^{232}Th, pre-Rn	3212 $\pm$ 225	3250 $\pm$ 90	-1.17
^{238}U, full series	79.08 $\pm$ 6.33	78 $\pm$ 6	1.38
^{238}U, pre-Rn	78.42 $\pm$ 6.27	78 $\pm$ 6	0.54
^{235}U, full series	3.56 $\pm$ 0.43	3.6 $\pm$ 3.2	-1.11
^{235}U, pre-Rn	3.49 $\pm$ 0.42	3.6 $\pm$ 3.2	-3.06
^{40}K	5.75 $\pm$ 0.58	6.3 $\pm$ 3.2	-8.73

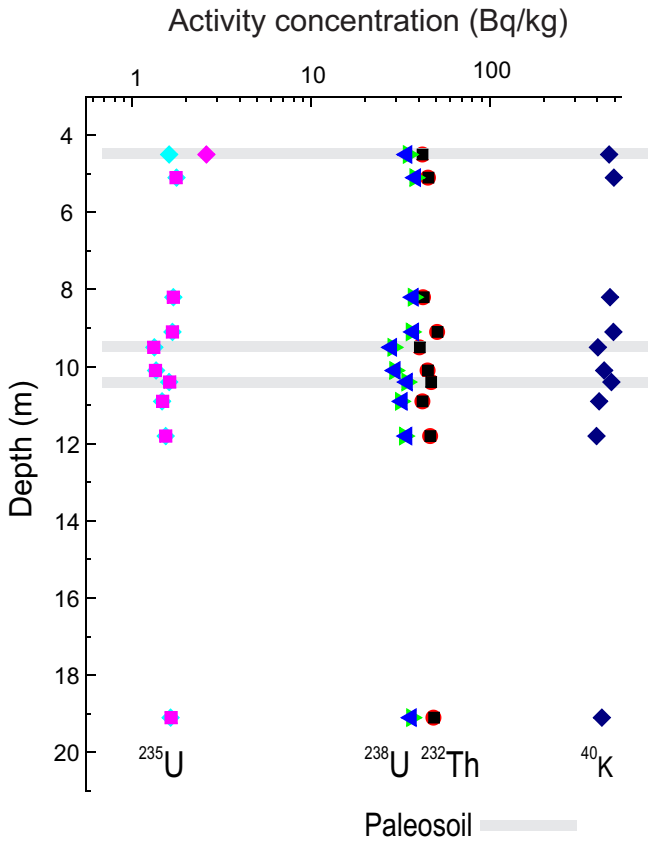

Fig. 1 – Vertical profile of activity concentrations of all four category of radionuclides. In the case of natural series of ^{232}Th, ^{238}U as well as ^{235}U, the data corresponding to full series as well as to pre-radon subseries are almost overlapped on graph. To illustrate an the same graph the activity concentrations of all four kind of radioelements, we have used a semilogarithmic plot.

The resulting activity concentrations of natural radioactive elements of Dobrudja loess and paleo-soil, reproduced in Table 6 and illustrated in Fig. 1 allowed us to make some remarks.

The first remarks concern the precision of experimental determination. In all cases, the total uncertainty varied between 7 and 12 %, the maximum being observed in the case of ^{235}U series, fact well explained by the relative lower intensity of corresponding gamma ray line, a consequence of its reduced isotopic abundance.

A second remark points toward the existence of radioactive equilibrium within all radioactive natural series, as the activity concentration corresponding to pre-Rn

and full series are coincident within the experimental uncertainties. From geologic point o view, this peculiarity could be interpreted as an absence of significant alteration processes during the loess deposits formation.

A third remarks is related with the absence of a statistically significant difference between loess and paleo-soil. Indeed, no systematic difference regarding the activity concentration of all investigated radionuclides between loess and paleo-soil was remarked, suggesting the same origin for the material which formed the entire loess deposit as well as a mild climate during interglacial when it is supposed the

Table 6

Numerical values of the activity concentrations (Λ_c) (in Bq/kg) of investigate samples.

Sample	Nuclide	Λ_c	Sample	Nuclide	Λ_c
G 1-2	$^{232}\mathrm{Th}_{fs}$	42.08 ± 2.95	G 5	$^{232}\mathrm{Th}_{fs}$	45.12 ± 3.16
(paleo-soil)	$^{232}\mathrm{Th}_{Rn}$	41.97 ± 2.94	(loess)	$^{232}\mathrm{Th}_{Rn}$	44.88 ± 3.14
	$^{238}\mathrm{U}_{fs}$	35.05 ± 2.80		$^{238}\mathrm{U}_{fs}$	29.43 ± 2.35
	$^{238}\mathrm{U}_{Rn}$	34.29 ± 2.74		$^{238}\mathrm{U}_{Rn}$	29.50 ± 2.36
	$^{235}\mathrm{U}_{fs}$	1.61 ± 0.19		$^{235}\mathrm{U}_{fs}$	1.36 ± 0.16
	$^{235}\mathrm{U}_{Rn}$	1.60 ± 0.19		$^{235}\mathrm{U}_{Rn}$	1.35 ± 0.16
	$^{40}\mathrm{K}$	465.1 ± 46.5		$^{40}\mathrm{K}$	436.34 ± 43.6
G 2	$^{232}\mathrm{Th}_{fs}$	45.40 ± 3.18	G 5-6	$^{232}\mathrm{Th}_{fs}$	47.00 ± 3.29
(loess)	$^{232}\mathrm{Th}_{Rn}$	45.09 ± 3.16	(paleo-soil)	$^{232}\mathrm{Th}_{Rn}$	47.03 ± 3.29
	$^{238}\mathrm{U}_{fs}$	38.15 ± 3.05		$^{238}\mathrm{U}_{fs}$	34.40 ± 2.75
	$^{238}\mathrm{U}_{Rn}$	38.39 ± 3.07		$^{238}\mathrm{U}_{Rn}$	34.54 ± 2.76
	$^{235}\mathrm{U}_{fs}$	1.77 ± 0.21		$^{235}\mathrm{U}_{fs}$	1.61 ± 0.19
	$^{235}\mathrm{U}_{Rn}$	1.76 ± 0.21		$^{235}\mathrm{U}_{Rn}$	1.62 ± 0.19
	$^{40}\mathrm{K}$	494.3 ± 49.4		$^{40}\mathrm{K}$	478.9 ± 47.9
G 3	$^{232}\mathrm{Th}_{fs}$	42.69 ± 2.99	G 6	$^{232}\mathrm{Th}_{fs}$	42.08 ± 2.95
(loess)	$^{232}\mathrm{Th}_{Rn}$	42.31 ± 2.96	(loess)	$^{232}\mathrm{Th}_{Rn}$	41.97 ± 2.94
	$^{238}\mathrm{U}_{fs}$	37.36 ± 2.99		$^{238}\mathrm{U}_{fs}$	31.69 ± 2.54
	$^{238}\mathrm{U}_{Rn}$	37.23 ± 2.98		$^{238}\mathrm{U}_{Rn}$	32.32 ± 2.59
	$^{235}\mathrm{U}_{fs}$	1.70 ± 0.20		$^{235}\mathrm{U}_{fs}$	1.47 ± 0.18
	$^{235}\mathrm{U}_{Rn}$	1.70 ± 0.20		$^{235}\mathrm{U}_{Rn}$	1.48 ± 0.18
	$^{40}\mathrm{K}$	470.9 ± 47.1		$^{40}\mathrm{K}$	409.1 ± 40.9
G 4	$^{232}\mathrm{Th}_{fs}$	50.99 ± 3.57	G 7	$^{232}\mathrm{Th}_{fs}$	46.54 ± 3.26
(loess)	$^{232}\mathrm{Th}_{Rn}$	50.75 ± 3.55	(loess)	$^{232}\mathrm{Th}_{Rn}$	46.37 ± 3.25
	$^{238}\mathrm{U}_{fs}$	36.37 ± 2.91		$^{238}\mathrm{U}_{fs}$	33.34 ± 2.67
	$^{238}\mathrm{U}_{Rn}$	37.44 ± 3.00		$^{238}\mathrm{U}_{Rn}$	34.29 ± 2.74
	$^{235}\mathrm{U}_{fs}$	1.68 ± 0.20		$^{235}\mathrm{U}_{fs}$	1.54 ± 0.18
	$^{235}\mathrm{U}_{Rn}$	1.68 ± 0.20		$^{235}\mathrm{U}_{Rn}$	1.54 ± 0.18
	$^{40}\mathrm{K}$	491.8 ± 49.2		$^{40}\mathrm{K}$	395.4 ± 39.5

Continues on the next page

Table 6

Continuation from precedent page

Sample	Nuclide	Λ_c	Sample	Nuclide	Λ_c
G 4-5	$^{232}Th_{fs}$	40.63 ± 2.84	G 8	$^{232}Th_{fs}$	48.83 ± 3.42
(paleo-soil)	$^{232}Th_{Rn}$	40.41 ± 2.83	(paleo-soil)	$^{232}Th_{Rn}$	48.41 ± 3.39
	$^{238}U_{fs}$	28.77 ± 2.30		$^{238}U_{fs}$	36.59 ± 2.93
	$^{238}U_{Rn}$	28.18 ± 2.25		$^{238}U_{Rn}$	36.31 ± 2.90
	$^{235}U_{fs}$	1.33 ± 0.16		$^{235}U_{fs}$	1.64 ± 0.20
	$^{235}U_{Rn}$	1.32 ± 0.16		$^{235}U_{Rn}$	1.65 ± 0.20
	^{40}K	402.6 ± 40.3		^{40}K	423.6 ± 42.4

The superscripts $_{fs}$ and $_{Rn}$ stand for "full series" and "pre-radon" respectively.

paleo-soil was generated.

A fourth remark is based on the results of a Principal Component Analysis performed on all experimental data and illustrated in Fig. 2 by a 2D plot of Principal component two *versus* principal component one. This graph shows that in the case of each of natural radioactive series, the point corresponding to the full series practically coincide with those of pre-radon subseries, thus confirming once more the existing radioactive equilibrium. Moreover, on the same graph, the points corresponding to ^{238}U and ^{235}U tends to group by forming a cluster, far away with respect to ^{232}Th and ^{40}K points respectively. This peculiarity could signify the existence within loess and paleo-soile of more mineral fractions, each of them with a different content of natural radioactive element.

Based on these experimental results, on eq. (2) as well as on the dose-rate conversion factors [19] it was possibly to calculate, for each group of samples, the

Table 7

Numerical value of annual dose rate for the South-eastern Dobrudja loes and paleo-soils

Sample	Depth (m)	Dose rate (mGy/y)	Sample	Depth (m)	Dose rate (mGy/y)
G 1-2 (paleo-soil)	4.5	2.868 ± 0.430	G5 (loess)	10.1	2.678 ± 0.402
G 2 (loess)	5.1	3.064 ± 0.460	G 5-6 (paleo-soil)	10.4	2.930 ± 0.440
G 3 (loess)	8.2	2.901 ± 0.435	G 6 (loess)	10.9	2.582 ± 0.387
G 4 (loess)	9.1	3.193 ± 0.479	G 7 (loess)	11.8	2.685 ± 0.403
G 4-5 (paleo-soil)	9.5	2.490 ± 0.374	G 8 (paleo-soil)	19.1	2.815 ± 0.422

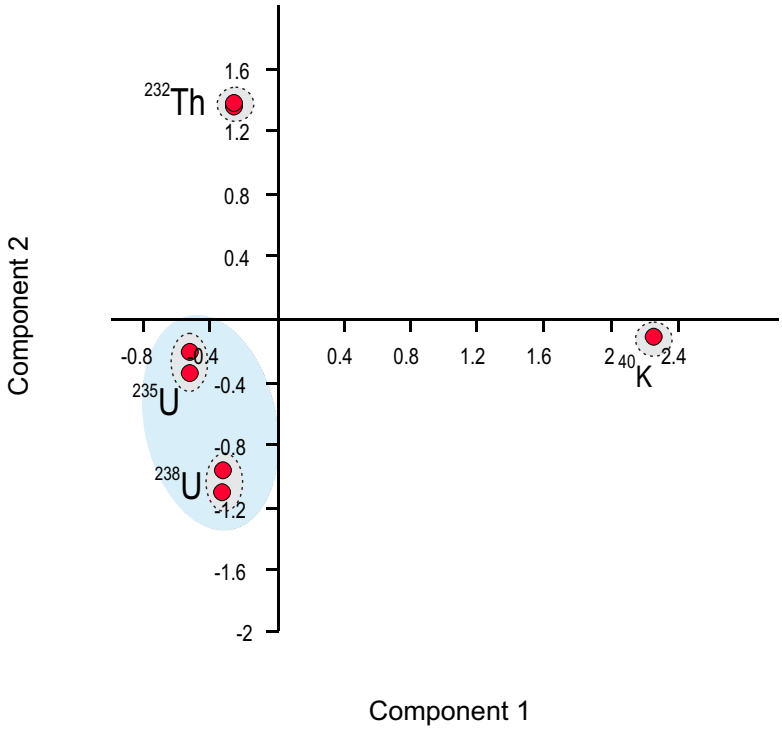

Fig. 2 – A 2D PCA plot of Principal component 1 *versus* Principal component 2 illustrating the radioactive equilibrium existing within each radioactive series as well as the difference between hosting minerals.

annual dose rate (see Table 7). As expected, the numerical value of dose rate reflect the steadiness of radiometric determinations so that the annual dose debit varied in a relatively narrow interval between 2.49 and 3.19 mGy/y, *i.e.* about 20%, close to the experimental value reported for similar loess deposits from Eastern Europe, Central and Eastern Asia [24–34] excepting South America, where the prevalence of volcanic dust determined a slightly higher value [35] (table 8). At the same time, these date confirm the relative uniformity of the chemical composition of Eurasian loess, as previously suggested by the Rare Earth Elements pattern, a typical one for the Upper Continental Crust [36]. It should be remarked that our data include also the contribution of cosmic ray background calculated according to [12, 13].

With these amendments, the numerical values of annual dose rate could be considered very useful for the future age determination of the Dobrudja loess deposits.

Table 8

Numerical value of annual dose rate (DR) for loess as well as paleo-soil reported in literature and used for TL and OSL geochronology.

Locality	DR (mGy/y)	Remarks	Ref.
Mostistea lake SE Romania	2.63 - 2.90	-	[24]
Erdutsko brdo Croatia	2.90 - 4.68	-	[25]
Stari Slankamen Vojvodina (Serbia)	3.09 - 3.87	-	[26]
Crvenka Vojvodina (Serbia)	2.98 - 4.05 2.55 - 3.71	feldspar quartz	[27]
Tokaj Hungary	3.37 - 3.87	-	[28]
Sutto Hungary	1.94 - 3.38	-	[29]
Biay Koci Streletzin, Poland	2.44 3.00	-	[30]
Boynychi (Volyn Upland) Ukraine	2.93 3.20	-	[31]
Darai Kalon/Chashmanigar Tadjikistan	2.68 - 4.18	-	[32]
Zhongjiacai, Tuxiangdao, Le Du Western China loess plateau	2.92 3.57	-	[33]
Luochuan Shaanxi Province, China	3.14 - 3.58	-	[34]
Tafi del Valle Tucumán, Argentina	4.79 - 5.18	-	[35]

4. CONCLUDING REMARKS

The direct gamma spectrometric determination of the activity concentration of the main natural radioactive elements was performed on ten samples of loess and paleo-soil collected from the South-Eastern Dobrudja loess deposits, near the village of Costinesti. The main purpose of this study was to calculate the local value of dose rates, absolute necessary for further TL age determination of loess deposit. All determinations were performed by taking into account the influence of the main spectrometric interferences so that to minimize their influence.

The accuracy of radiometric determination was checked by a paired t-test applied to IAEA-RGTh-1 certified reference material that gave for the t parameter a value of -0.011 at $p > 0.991$, confirming in this way the coincidence between rec-

ommended and measured values of activity concentrations of the main natural radionuclides.

Applied to the considered samples, final estimations gave for annual dose rates values between 2.49 and 3.19 mG/y, in god concordance with similar measurements performed on different loess deposits from Eastern Europe, Asia and at some extent from South America.

REFERENCES

1. D.R. Muhs DR (2013), 11.9 Loess and its Geomorphic, Stratigraphic, and Paleoclimatic Significance in: Quaternary Treatise on Geomorphology (J. Shroder ed.), Vol. 11, pp.149-183, Elsevier, Amsterdam (2013).
2. B. Buggle, B. Glaser, L. Zöller , U. Hambach, S. Markovic, I. Glaser and N. Gerasimenko, Quatern. Sci. Rev. **27**, 1058 (2008); doi:10.1016/j.quascirev.2008.01.018
3. A.G. Wintle, A review of current research on TL dating of loess, Quatern. Sci. Rev. **9**, 385 (1990); doi:10.1016/0277-3791(90)90029-A
4. P. Van den Haute, M. Frechen, J.-P. Buylaert, D. Vandenberghe, and F. De Corte, Quatern. Sci. Rev. **22** 985, (2003); doi: 0.1016/S0277-3791(03)00023-4
5. X. Wang, Z. Yang, R. Lovlie, Z. Sun, J. Pei, A, Phys. Earth Planet. Int. 159: 109 (2006); doi:10.1016/j.pepi.2006.07.002
6. S.A. Arkhipova, Z.N. Gnibidenko, V.N. Shelkoplyas, Quatern. Int. **6871**, 13 (2000); doi:10.1016/S1040-6182(00)00029-X
7. M.J. Aitken, M.S Tite, and J. Reid, Nature, **202**, 1032 (1964).
8. M.J. Aitken, D.W.Zimmerman, and S.J. Fleming, Nature, **219**, 442 (1968).
9. V. Mejdahl, Archaeometry, **11**, 99 (1969).
10. A.G. Wintle, and D.J. Huntley, Canad. J. Earth Sci. **17**, 348 (1980).
11. A. Timar-Gabor, S. Vasiliniuc, D.A.G. Vandenberghe, D. Constantin, and C. Cosma, Rom. Rep. Phys. **63**, 929 (2011).
12. M.J. Aitken, *Thermoluminescence dating* (359 p., Academic Press, London, 1985).
13. J.R. Prescott, and J.T. Hutton, Rad. Meas. **23**, 497 (1994).
14. Z. Papp, Z. Dezso, and S. Daroczy, J. Radioanal. Nucl. Chem. **222**, 171 (1997); doi: 10.1007/BF02034265
15. M. Tzortzis, E. Svoukis, and H.Tsertos, Rad. Prot. Dos. **109**, 217 (2004); doi: 10.1093/rpd/nch300.
16. C.I. Cristache, O.G. Duliu, O.A. Culicov, M.V. Frontasyeva, C. Ricman, and M. Toma, Appl. Rad. Isot. **67**, 901 (2009); doi:10.1016/j.apradiso.2009.01.054
17. R.M. Tripathi, A.C. Patra, S. Mohapatra, S.K. Sahoo, A.V. Kumar, and V.D. Puranik, J. Radioanal. Nucl. Chem. **295**, 1829 (2013); doi:10.1007/s10967-012-2106-2
18. IAEA-RGTh-1, Thorium Ore IAEA Reference Products for Environment and Trade , IAEA, Vienna (2013), http://nucleus.iaea.org/rpst/Documents/rl_148.pdf (last accessed 18.03.2013).
19. S.E. Warren, Archaeometry **20**, 69 (1978); doi:10.1111/j.1475-4754.1978.tb00215.x
20. G. Guérin G, N. Mercier N, and G. Adamiec, Ancient TL **29**, 5 (2011).
21. S.Y.F. Chu, L.P. Ekstrm, and R.B. Firestone, The Lund/LBNL Nuclear Data Search (1999), http://nucleardata.nuclear.lu.se (last accessed 15.03.2013).
22. F. De Corte, H, Umans,D. Vandenberghe, A. De Wispelaere, and P. Van den Haute, Appl. Rad. Isot. **63**, 589 (2005); doi:10.1016/j.apradiso.2005.05.008

23. K.J.R. Rosman, and P.D.P Taylor, Pure Appl. Chem. **70**, 217 (1998); doi:10.1351/pac199870010217
24. S. Vasiliniuc, A. Timar-Gabor, D.A.G. Vandenberghe, G.C. Panaiotu, R.Cs. Begy, and C. Cosma, Geochronometria **38**, 34 (2011); doi: 10.2478/s13386-011-0007-8
25. L. Galovic, M. Frechen, J. Halamic, G. Durn, and M. Romic, Quatern. Int. **198**, 85 (2009); doi: 10.1016/j.quaint.2008.02.004
26. E.D. Schmidt, B. Machalett, S.B. Markovic, S. Tsukamoto, and M. Frechen, Quatern. Geochron. **5**, 137 (2010); doi:10.1016/j.quageo.2009.09.006
27. T. Stevens, S.B. Markovi, M. Zech, U. Hambach, and P. Sumegi, Dust deposition and climate in the Carpathian Basin over an independently dated last glacial - interglacial cycle, Quatern. Sci. Rev.**30**, 662 (2011); doi:10.1016/j.quascirev.2010.12.011
28. A.-K. Schatz, J-P Buylaert, A. Murray, T. Stevens and T. Scholten, Quatern. Geochron. **10**, 68 (2011); doi: 10.1016/j.quageo.2012.02.018
29. A. Novothny, E. Horváth, L. Wacha, and C. Rolf, Quatern. Intern. **234**, 75 (2010); doi: 10.1016/j.quaint.2010.08.002
30. P. Moska, G. Adamiec, and Z. Jary, Geochronometria **38**, 162 (2011); doi: 10.2478/s133860110013
31. J. Kusiak, M. Lanczont, and A.B. Bogucki, Geochronometria **39**, 84 (2012); doi: 10.2478/s13386-011-0054-1
32. M. Frechen, and A.E. Dodonov, Geol. Rund. **87**, 2-20 (1998); doi:10.1007/s005310050185
33. J.P. Buylaert, A.B. Murray, D. Vandenberghe, M. Vriend, D. De Corte, and P. Van den Haute, Quatern. Geochron. **3**, 99 (2008); doi:10.1016/j.quageo.2007.05.003
34. Z. Lai, J. Asian Earth Sci. **37**,176 (2010); doi: 10.1016/j.jseaes.2009.08.003
35. B. Carter-Stiglitz, S.K. Banerjee, A.Gourlan, E. Oches, Palaeo., Palaeo., Palaeo. **239**, 45 (2006); doi:10.1016/j.palaeo.2006.01.008
36. S.R. Taylor and S.M. McLennan, *The Continental Crust: Its Composition and Evolution* (312 p., Blackwell, Oxford, 1991).